

ORIGINAL RESEARCH

Generalized frequency estimator with rational combination of three spectrum lines

 Benjamin Gigleux^{1,2,3}  | François Vincent^{2,3}  | Eric Chaumette^{2,3} 
¹SpaceAble, Lacombe, France²Department DEOS, ISAE-SUPAERO, University of Toulouse, Toulouse, France³Telecommunication for Space and Aeronautics (TéSA) Laboratory, Toulouse, France**Correspondence**

Benjamin Gigleux, SpaceAble, Lacombe, 19500 Curemonte, France.

Email: benjamin.gigleux@spaceable.org**Funding information**

SpaceAble

Abstract

The popular Discrete Fourier Transform (DFT) is known to be a sub-optimal frequency estimation technique for a finite transform length. In order to approach the Cramer-Rao Lower Bound (CRLB), many refinement techniques have been considered, but little considering both zero padding or tapering, also known as windowing or apodisation. In this paper, a frequency estimator with closed-form combination of three DFT samples is generalized to zero padding and tapered data within the class of cosine windowing. Root Mean Squared Error (RMSE) is shown to approach the CRLB in the case of a single tone signal with additive white Gaussian noise. Compared to state-of-the-art techniques, the proposed algorithm improves the frequency RMSE up to 1 dB when using significant zero-padding lengths ($K \geq 2N$) and for small to moderate SNR, which is the most challenging case for practical radar applications.

KEYWORDS

frequency estimation, discrete Fourier transforms, radar signal processing

1 | INTRODUCTION

Frequency estimation is at stake in services such as telecommunication or Global Navigation Satellite System (GNSS), to cite a few. Most of the time, the Doppler frequency of a signal needs to be estimated, so that the problem can be simplified to a single tone estimation with unknown amplitude and frequency, in additive noise. This noise is usually assumed to be white and Gaussian. In such a situation, the Maximum Likelihood Estimator (MLE), which achieves asymptotically the Cramer-Rao Lower Bound (CRLB), consists in maximising the so-called periodogram [1]. Unfortunately, this maximisation process hardly complies with computation resources in embedded systems. Consequently, the Discrete Fourier Transform (DFT) is regularly implemented and has adequate accuracy in many applications. DFT simply consists in computing the periodogram on a finite and uniform set of frequencies. Nevertheless, this simple and widely used solution is shown to have a mean square error convergence in the order of $O(N^{-2})$ [2], whereas the CRLB is in $O(N^{-3})$ [3], where N stands for the data length. When a more accurate frequency

estimation is required, zero padding may be considered to interpolate the periodogram. However, especially when considering embedded systems, both the computational resources and the memory size may prevent from using DFT with large zero padding.

Hence, many sub-optimal but computationally efficient algorithms have been proposed over the last 50 years. Among this huge quantity of schemes, the class of the displacement-based techniques, also known as Amplitude Estimation techniques [3–19], exhibits one of the best precision-to-computational complexity ratios. Indeed, these 2-step algorithms first consist in a coarse frequency estimation based on the DFT followed by a fine frequency estimation based on a few DFT samples (typically 3) around the maximum frequency bin, where up to 85% of the tone energy is concentrated [9]. The main advantage of these kinds of algorithms relies on the closed-form formulation of the second step, so that the computational load is marginal compared to the first step, namely the DFT. Some of the most popular displacement-based techniques are summarised hereafter:

This is an open access article under the terms of the Creative Commons Attribution-NonCommercial-NoDerivs License, which permits use and distribution in any medium, provided the original work is properly cited, the use is non-commercial and no modifications or adaptations are made.

© 2022 The Authors. *IET Radar, Sonar & Navigation* published by John Wiley & Sons Ltd on behalf of The Institution of Engineering and Technology.

- In [3], Rife and Boorstyn derive a secant interpolation method.
- In [10], Brown III et al. use a quadratic interpolation of the periodogram main peak to derive the interpolation coefficients.
- In [11], Rife and Vincent determine the frequency from the amplitude of three DFT samples. However, the algorithm exhibits large Mean Squared Error (MSE) when the normalized frequency is rational.
- In [13], Quinn modifies [11] to solve the above-mentioned rational frequency issue. The asymptotic MSE of this algorithm is shown to vary between $(1.6449 \times \text{CRLB})$ and $(1.0088 \times \text{CRLB})$, depending on the gap between the true frequency and the DFT bins.
- In [15], Quinn extends the algorithm defined in [13] to tapered data with Hanning or Hamming window.
- In [17], Duda proposes an algorithm for tapered data with arbitrary windows.
- In [18], Jacobsen and Kootsookos improve a simple Early-Minus-Late (EML) estimator, formerly defined from fitting a parabola to three DFT samples, and then adjust the estimator to tapered data.
- In [19], Yang and Wei derive an EML estimator for non-tapered data in the case where the zero padding is twice the DFT length. The asymptotic MSE is shown to reach between $(1.1014 \times \text{CRLB})$ and $(1.0147 \times \text{CRLB})$.

Nevertheless, none of the displacement-based techniques, cited above, fully covers the practical needs of radar applications, which possibly requires both zero padding and tapering. More precisely, zero padding may be required either to reach a DFT length that equals a power of 2, and therefore implement DFT as split-radix FFT algorithm [22], or to mitigate the impact of spectral leakage, also known as scalloping losses, in the radar link budget. Tapering may also be required to mitigate spectral leakage in the radar link budget [23] or to lower the secondary lobes of targets for the purpose of unmasking a small target [24].

To the best of the authors' knowledge, the only refinement frequency estimation technique that manages both zero padding and tapering is defined by Candan in [21]. Indeed, Candan first derives an estimator in [20] that removes the bias from the estimator proposed in [18]. Then, this estimator is extended to zero padding and tapering in [21] and therefore complies with practical needs of radar applications.

The goal of this paper is to propose a new frequency estimation scheme, which also manages both zero padding and tapering. To this end, the work of Yang and Wei [19] is extended to the case of both zero-padded and tapered data.

The remaining of this paper is organised as follows. The model at hand is introduced in Section 2. Then, based on Yang and Wei's approach, the interpolation coefficients are derived in Section 3 for zero padding and tapering. More precisely, the popular and general class of cosine tapered windows is

considered in this paper. In addition, a performance evaluation of the new scheme is conducted in Section 4. Finally, the performance is compared with Quinn's estimators [13, 15] and Candan's estimator [21] in Section 5 and concluding remarks are given in Section 6.

2 | MODEL AND NOTATIONS

A complex single tone is considered. This signal is sampled at a constant sampling rate, so that N samples are available:

$$y[n] = x[n] + \varepsilon[n] = Ae^{j\omega n} + \varepsilon[n], \quad n \in \llbracket 0, N-1 \rrbracket \quad (1)$$

where A and ω are, respectively, the complex amplitude and the pulsation of the signal. Both parameters are assumed to be constant and unknown. $\varepsilon[n]$ are independent white Gaussian noise samples with zero mean and variance σ^2 .

A zero-padded version of the DFT of this signal is considered. Hence, let $K \geq 2N$ be the DFT length of the signal, so that $(K - N)$ be the length of zero padding. Then, the DFT of $y[n]$ is defined as follows:

$$\begin{aligned} Y[k] &= X[k] + \varepsilon[k] \\ &= \sum_{n=0}^{N-1} (x[n] + \varepsilon[n])e^{-j\omega_k n}, \quad k \in \llbracket 0, K-1 \rrbracket \end{aligned} \quad (2)$$

where

$$\omega_k = 2\pi \frac{k}{K} \quad (3)$$

As already explained in the introduction, a tapered version of the DFT is considered in this paper to mitigate possible sidelobes interference. To this end, the class of cosine windows is recalled and can be expressed as the linear combination of DFT of non-tapered data as

$$\begin{aligned} \tilde{Y}[k] &= \sum_{m=0}^{M-1} \frac{H[m]}{2} \{Y[k-m] + Y[k+m]\} \\ &= \sum_{m=0}^{M-1} \sum_{n=0}^{N-1} H[m] \cos\left(2\pi m \frac{n}{N}\right) (x[n] + \varepsilon[n])e^{-j\omega_k n} \end{aligned} \quad (4)$$

where $\{H[m], m \in \llbracket 0, M-1 \rrbracket\}$ are the Fourier cosine coefficients of the window and are given in Table 1 for usual windows [23].

3 | FREQUENCY ESTIMATION

Based on the model defined in Section 2, the proposed frequency estimation is now based on a two-step procedure, similar to all displacement-based estimation techniques.

TABLE 1 :Coefficients of usual windows

Window	H [0]	H [1]	H [2]	H [3]
Rectangular	+1	0	0	0
Hanning	+25/46	-21/46	0	0
Hamming	+0.5	-0.5	0	0
Blackman-harris	+0.35875	0.48829	+0.14128	-0.01168

3.1 | Coarse estimation

The initial step is the standard coarse estimation using the zero-padded DFT maximisation, simply:

$$k_0 = \operatorname{argmax} \left\{ |\tilde{Y}[k]|^2, k \in \llbracket 0, K-1 \rrbracket \right\} \quad (5)$$

3.2 | Fine estimation

The second step is based on a mean squared error minimisation. The criterion to be minimised is the difference between the measured DFT power and a DFT power model, computed on the 3 samples near the main DFT peak, namely k_0 . Let us introduce:

$$(\hat{\gamma}, \hat{\alpha}) = \operatorname{argmin} \{J(\gamma, \alpha)\} \quad (6)$$

$$J(\gamma, \alpha) = \sum_{k=k_0-1}^{k_0+1} \left(|\tilde{Y}[k]|^2 - \gamma^2 \tilde{P}(\omega_k - \omega_{k_0} - \alpha) \right)^2 \quad (7)$$

where γ is an estimate of the signal power (i.e. $|A|^2$) while $\alpha = \omega - \omega_{k_0}$ is the pulsation residual error with respect to the first step estimation, namely $\omega_{k_0} = 2\pi(k_0/K)$. Finally, $\tilde{P}(\delta)$ is the normalized power spectrum in a noiseless case (i.e. $|X|^2/|A|^2$), where δ is the pulsation offset from the spectrum peak power. $\tilde{P}(\delta)$ is shown to be

$$\tilde{P}(\delta) = \left| \sum_{m=0}^{M-1} \frac{H[m]}{2} \left(\frac{1 - e^{j(\delta - 2\pi \frac{m}{K})N}}{1 - e^{j(\delta - 2\pi \frac{m}{K})}} + \frac{1 - e^{j(\delta + 2\pi \frac{m}{K})N}}{1 - e^{j(\delta + 2\pi \frac{m}{K})}} \right) \right|^2 \quad (8)$$

In order to obtain a closed-form formulation of α , and given that α is small, a first order Taylor series expansion of \tilde{P} is used

$$\begin{aligned} \tilde{P}(\omega_k - \omega_{k_0} - \alpha) &= \tilde{P}(\omega_k - \omega_{k_0}) + \alpha \times \left. \frac{\partial \tilde{P}(\delta)}{\partial \delta} \right|_{\delta=\omega_k - \omega_{k_0}} \\ &= \tilde{P}(\omega_k - \omega_{k_0}) + \alpha \times \tilde{P}'(\omega_k - \omega_{k_0}) \end{aligned} \quad (9)$$

Then, introducing new and equivalent parameters

$$\begin{cases} a = \gamma \\ b = \gamma\alpha \end{cases} \quad (10)$$

The minimisation solution is shown to be

$$\begin{cases} \left(\frac{\partial J}{\partial a} = 0 \right) \Rightarrow \hat{a} = \frac{\sum_{k=k_0-1}^{k_0+1} |\tilde{Y}[k]|^2 \tilde{P}(\omega_k - \omega_{k_0})}{\sum_{k=k_0-1}^{k_0+1} \left(\tilde{P}(\omega_k - \omega_{k_0}) \right)^2} \\ \left(\frac{\partial J}{\partial b} = 0 \right) \Rightarrow \hat{b} = \frac{\sum_{k=k_0-1}^{k_0+1} |\tilde{Y}[k]|^2 \tilde{P}'(\omega_k - \omega_{k_0})}{\sum_{k=k_0-1}^{k_0+1} \left(\tilde{P}'(\omega_k - \omega_{k_0}) \right)^2} \end{cases} \quad (11)$$

while the residual frequency error can be estimated as follows:

$$\hat{\alpha} = \frac{\hat{b}}{\hat{a}} \quad (12)$$

Observing that function $\tilde{P}(\delta)$ is even, and as a consequence $\tilde{P}'(\delta)$ is odd, then Equation (12) can be simplified. Therefore, the fine estimation bias of the frequency is shown to be

$$\hat{\alpha} = - \frac{|\tilde{Y}[k_0-1]|^2 - |\tilde{Y}[k_0+1]|^2}{u \left(|\tilde{Y}[k_0-1]|^2 + |\tilde{Y}[k_0+1]|^2 \right) + v |\tilde{Y}[k_0]|^2} \quad (13)$$

with

$$\begin{cases} u = \frac{2\tilde{P}'\left(\frac{2\pi}{K}\right)\tilde{P}\left(\frac{2\pi}{K}\right)}{\tilde{P}(0)^2 + 2\tilde{P}\left(\frac{2\pi}{K}\right)^2} \\ v = u \frac{\tilde{P}(0)}{\tilde{P}\left(\frac{2\pi}{K}\right)} \end{cases} \quad (14)$$

Finally, the frequency estimator is given by

$$\hat{\omega} = 2\pi \frac{k_0}{K} + \hat{\alpha} \quad (15)$$

This closed-form and simple expression generalises the frequency estimation proposed in [19] in the case of a zero padding with an arbitrary length and for any kind of tapered data within the class of cosine windows.

4 | PERFORMANCE EVALUATION

In order to evaluate the estimation performance of the proposed scheme, U and V are introduced, corresponding to both the numerator and the denominator of $\hat{\alpha}$ in Equation (13), in a noiseless case, namely:

$$\begin{cases} U = |\tilde{X}[k_0 - 1]|^2 - |\tilde{X}[k_0 + 1]|^2 \\ V = u\left(|\tilde{X}[k_0 - 1]|^2 + |\tilde{X}[k_0 + 1]|^2\right) + v|\tilde{X}[k_0]|^2 \end{cases} \quad (16)$$

The corresponding measurement errors $\hat{\delta}_U$ and $\hat{\delta}_V$ are now defined, when considering the noisy data, and assuming that the first step estimation (DFT maximisation) is correct

$$\begin{cases} U + \hat{\delta}_U = |\tilde{Y}[k_0 - 1]|^2 - |\tilde{Y}[k_0 + 1]|^2 \\ V + \hat{\delta}_V = u\left(|\tilde{Y}[k_0 - 1]|^2 + |\tilde{Y}[k_0 + 1]|^2\right) + v|\tilde{Y}[k_0]|^2 \end{cases} \quad (17)$$

so that the estimation error on $\hat{\alpha}$ can be expressed as

$$\hat{\alpha} - \alpha = \frac{U + \hat{\delta}_U}{V + \hat{\delta}_V} - \frac{U}{V} \quad (18)$$

The latest can be approximated as follows, when both $\hat{\delta}_U$ and $\hat{\delta}_V$ are small

$$\hat{\alpha} - \alpha \simeq \frac{\hat{\delta}_U}{V} - \frac{U\hat{\delta}_V}{V^2} \quad (19)$$

As a consequence, the proposed estimator is asymptotically unbiased, namely

$$E[\hat{\alpha} - \alpha] \sim \frac{U(2u + v)\tilde{\Sigma}_0^2}{V^2} \sim 0 \quad (20)$$

where $\tilde{\Sigma}_0^2$ represents the noise variance whose expression is given in Equation (26). The Mean Squared Error (MSE) of the proposed estimator can be expressed as follows:

$$E[(\hat{\alpha} - \alpha)^2] \sim \frac{1}{V^2} E[\hat{\delta}_U^2] - \frac{2U}{V^3} E[\hat{\delta}_U \hat{\delta}_V] + \frac{U^2}{V^4} E[\hat{\delta}_V^2] \quad (21)$$

Given that

$$|\tilde{Y}[k]|^2 \sim |\tilde{X}[k]|^2 + 2\Re\{\tilde{X}[k]\tilde{\varepsilon}[k]\} \quad (22)$$

the variances and covariance of measurement errors $\hat{\delta}_U$ and $\hat{\delta}_V$ can now be written

$$\begin{aligned} E[\hat{\delta}_U^2] &\sim 2\left(|\tilde{X}[k_0 - 1]|^2 + |\tilde{X}[k_0 + 1]|^2\right)\tilde{\Sigma}_0^2 \\ &\quad - 4\Re\{\tilde{X}^H[k_0 - 1]\tilde{X}[k_0 + 1]\tilde{\Sigma}_2^2\} \end{aligned} \quad (23)$$

$$\begin{aligned} E[\hat{\delta}_U \hat{\delta}_V] &\sim 2u\left(|\tilde{X}[k_0 - 1]|^2 - |\tilde{X}[k_0 + 1]|^2\right)\tilde{\Sigma}_0^2 \\ &\quad + 2v\Re\left\{\left(\tilde{X}^H[k_0 - 1]\tilde{X}[k_0] \right. \right. \\ &\quad \left. \left. - \tilde{X}[k_0 + 1]\tilde{X}^H[k_0]\right)\tilde{\Sigma}_1^2\right\} \end{aligned} \quad (24)$$

$$\begin{aligned} E[\hat{\delta}_V^2] &\sim 2\left(u^2|\tilde{X}[k_0 - 1]|^2 + v^2|\tilde{X}[k_0]|^2 \right. \\ &\quad \left. + u^2|\tilde{X}[k_0 + 1]|^2\right)\tilde{\Sigma}_0^2 \\ &\quad + 4uv\Re\left\{\left(\tilde{X}^H[k_0 - 1]\tilde{X}[k_0] \right. \right. \\ &\quad \left. \left. - \tilde{X}[k_0 + 1]\tilde{X}^H[k_0]\right)\tilde{\Sigma}_1^2\right\} \\ &\quad + 4u^2\Re\left\{\tilde{X}^H[k_0 - 1]\tilde{X}[k_0 + 1]\tilde{\Sigma}_2^2\right\} \end{aligned} \quad (25)$$

where $\{\tilde{\Sigma}_k^2, k \in \{0, 1, 2\}\}$ is the noise covariance matrix that is:

$$\begin{aligned} \tilde{\Sigma}_k^2 &= E[\tilde{\varepsilon}[l]\tilde{\varepsilon}^H[l+k]] \\ &= \frac{\sigma^2}{4} \sum_{m_1=0}^{M-1} \sum_{m_2=0}^{M-1} H[m_1]H[m_2] \\ &\quad \times \begin{cases} 1 - e^{-j2\pi\left(\frac{k}{K} + \frac{m_1}{N} + \frac{m_2}{N}\right)N} \\ 1 - e^{-j2\pi\left(\frac{k}{K} + \frac{m_1}{N} + \frac{m_2}{N}\right)} \end{cases} \\ &\quad + \frac{1 - e^{-j2\pi\left(\frac{k}{K} + \frac{m_1}{N} - \frac{m_2}{N}\right)N}}{1 - e^{-j2\pi\left(\frac{k}{K} + \frac{m_1}{N} - \frac{m_2}{N}\right)}} \\ &\quad + \frac{1 - e^{-j2\pi\left(\frac{k}{K} - \frac{m_1}{N} - \frac{m_2}{N}\right)N}}{1 - e^{-j2\pi\left(\frac{k}{K} - \frac{m_1}{N} - \frac{m_2}{N}\right)}} \\ &\quad + \frac{1 - e^{-j2\pi\left(\frac{k}{K} - \frac{m_1}{N} + \frac{m_2}{N}\right)N}}{1 - e^{-j2\pi\left(\frac{k}{K} - \frac{m_1}{N} + \frac{m_2}{N}\right)}} \end{cases} \quad (26)$$

Observing Equation (21), one can notice that the unknown initial phase of the signal, namely $\arg\{A\}$, does not impact the Root Mean Squared Error (RMSE) of the estimator. This property is expected for any frequency estimator whose MSE is close to the CRLB, since the CRLB for frequency estimation of a single tone in additive white Gaussian noise does not depend on the signal phase [3]. To the contrary, the RMSE depends on the coarse error, namely $|\omega - \omega_{k_0}|$, which impacts the amplitude of the three DFT samples.

5 | NUMERICAL ASSESSMENTS

In order to assess the validity of the proposed estimator given by Equation (13), its RMSE is now evaluated using Monte-Carlo simulations (10, 000 runs). The RMSE is compared with the analytical RMSE given in Equation (21). For comparison purposes, both the RMSE and the associated analytical RMSE are normalized by the CRLB for frequency estimation of a single tone in additive white Gaussian noise [15]:

$$\sigma_{CRLB}^2 = \frac{\sigma^2}{|A|^2} \times \frac{6}{N(N^2 - 1)} \quad (27)$$

where $|A|^2/\sigma^2$ is the Signal-to-Noise Ratio (SNR).

The results are also compared to the asymptotic standard deviation for frequency estimation through the maximisation of the periodogram of tapered data, with either Hamming or Hanning windows [15]. The asymptotic standard deviation in the case of Blackman-Harris window is not available in the literature, to the best of the author's knowledge. Besides, one should note that Equation (27) also corresponds to the asymptotic standard deviation in the case of rectangular window [15].

First of all, it is reminded that the case $K = 2N$ with rectangular window corresponds to the technique in [19].

Secondly, the well-known MLE breakdown threshold [3, 9] can be observed in Figure 1 and Figure 2, where the RMSE dramatically departs from the CRLB under a given SNR. However, the simulated RMSE of the proposed algorithms is very close to the analytical RMSE calculated in

Section 4, in the asymptotic region. The gap between the RMSE and the CRLB of Equation (27) is somehow the price to pay to mitigate sidelobes thanks to tapering, which enables to lower ambiguities in a multiple targets scenario or to unmask a smaller target located in the sidelobes of a stronger target. Nevertheless, for cosine windows, the simulated RMSE remains very close to the specific asymptotic standard deviation calculated for each specific window [15], as shown on Figure 3.

Thirdly, one can observe a different behaviour depending on the residual frequency error after the coarse estimation, defined in Section 3.1. Indeed, unlike in Figure 1 where $|\omega - \omega_{k_0}|$ is close to 0, a progressive loss from the analytical RMSE can be observed in Figure 2 when $|\omega - \omega_{k_0}|$ is close to 0.5. This behaviour originates from the quadratic error, caused by the linearisation in Equation (9), that dominates the error budget in extremely high SNR when $|\omega - \omega_{k_0}|$ is large. However, this loss of performances in such a case only come up for large SNR where the performances are already very good. One should note that the same observations apply to other popular displacement-based techniques, unless the non-linearity is compensated through bias removal as in [15, 21].

Fourthly, the coarse estimation defined in Section 3.1 can be erroneous, especially at low SNR, while the analytical RMSE is given for a non-erroneous coarse estimation in Equation (21). This explains the small but observable discrepancies between the simulated RMSE and the analytical RMSE in Figure 3, especially when $|\omega - \omega_{k_0}|$ is close to 0.5 where spectral leakage is maximal. The same observation applies in Figures 4 and 5 where spectral leakage is higher at low zero padding (i.e. low K/N) and degrades the SNR. Coarse estimation also biases the overall estimation process at low SNR,

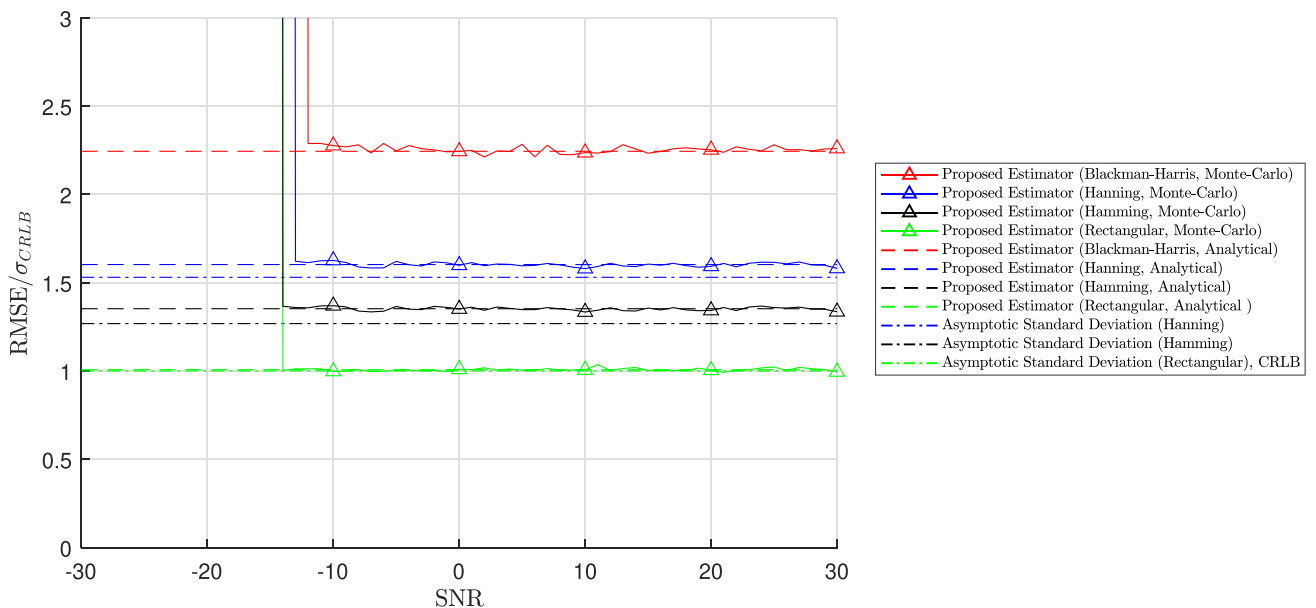


FIGURE 1 Performance of proposed estimator ($N = 1024$, $K = 2N$, $|\omega - \omega_{k_0}| = 0$)

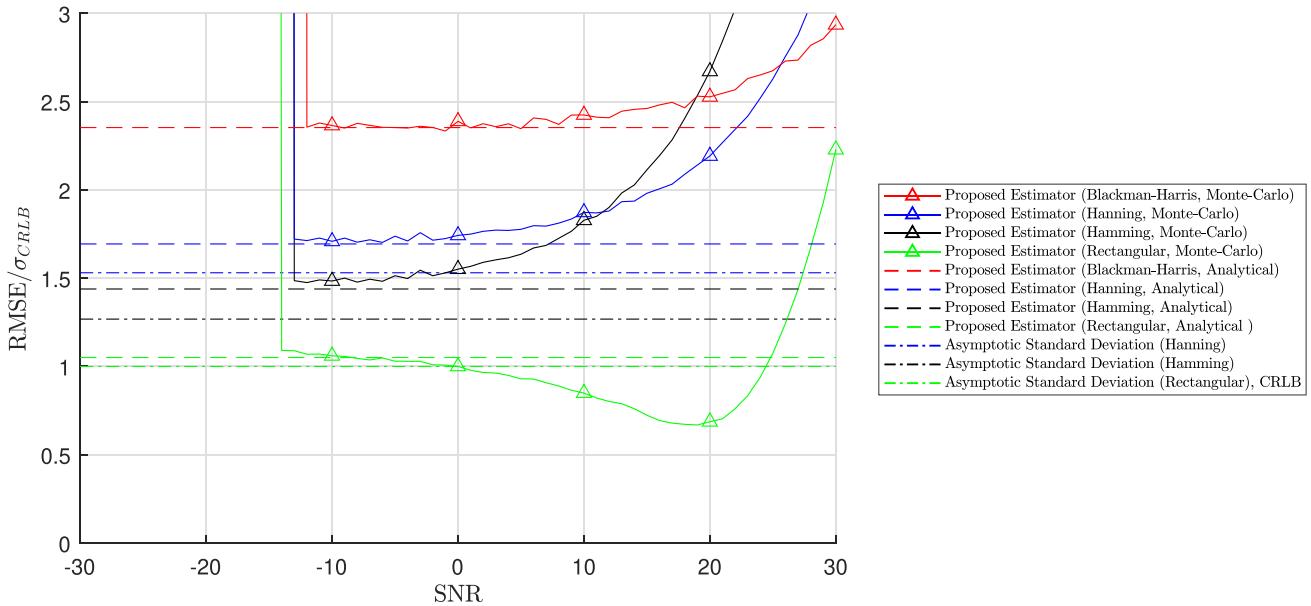


FIGURE 2 Performance of proposed estimator ($N = 1024$, $K = 2N$, $|\omega - \omega_{k_0}| = 0.5$)

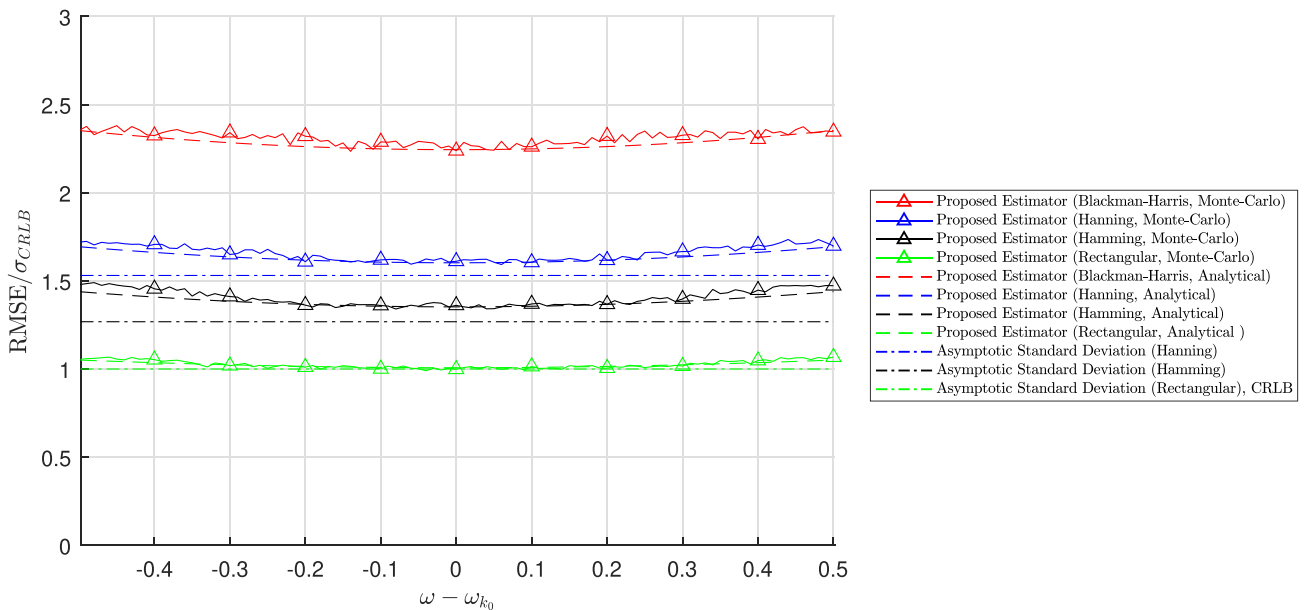


FIGURE 3 Performance of Proposed Estimator (Signal-to-Noise Ratio = -10 dB, $N = 1024$, $K = 2N$)

which explains why the RMSE can drop below the CRLB in Figures 2 and 5.

Moreover, an analysis with respect to the zero-padding length is proposed in Figures 4 and 5. Once again, the simulated RMSE is very close to the analytical RMSE and both approach the asymptotic standard deviation as soon as K is larger than 2 or 3 times the signal length, N .

To finish with, Figures 6–9 aim at comparing our proposed scheme with both of the best literature's algorithms, namely Quinn's [13, 15] and Candan's estimators [21]. Beyond the breakdown threshold (i.e. in the asymptotic

region), each marker represents the technique with the lowest maximum RMSE for different SNR and zero padding, and for different tapering windows. This comparison is conducted with different residual frequency error, $(\omega - \omega_{k_0})$, uniformly sampled (101 points) within the interval $[-0.5, +0.5]$. For each point, the RMSE is estimated using Monte-Carlo simulations (10, 000 runs). Then, each estimator is characterised by its maximum RMSE over the variations of the residual frequency error.

In addition, a background colour represents the improvement of the proposed method compared to Quinn's or

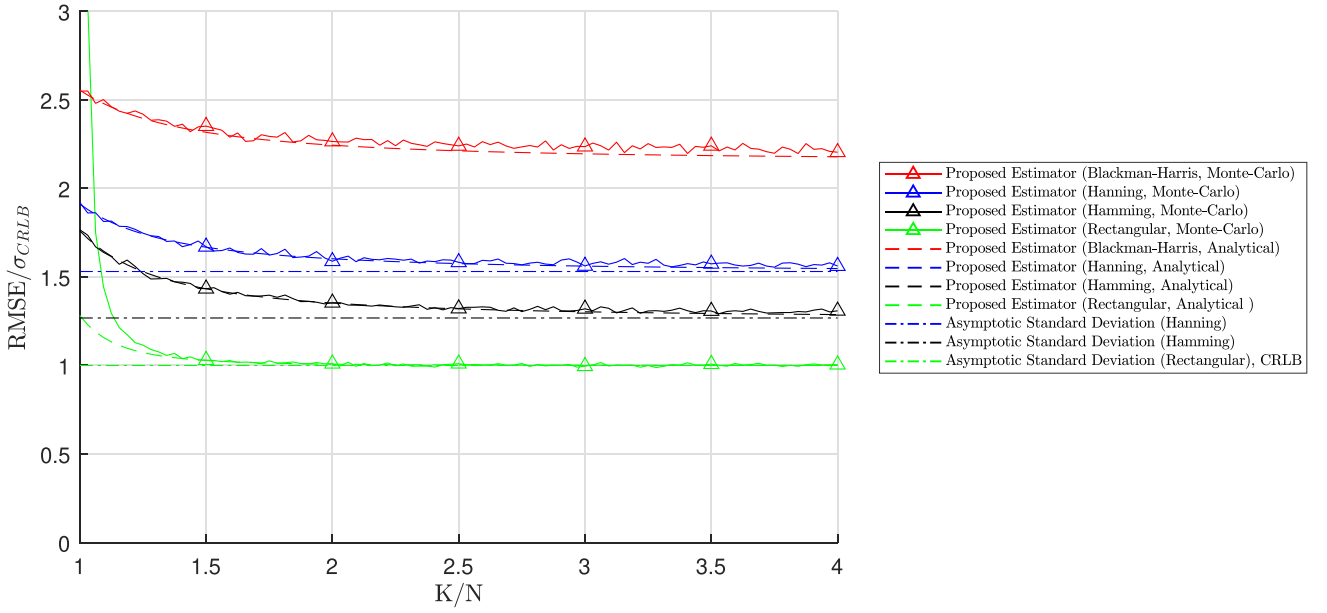


FIGURE 4 Performance of proposed estimator (Signal-to-Noise Ratio = -10 dB, $N = 1024$, $|\omega - \omega_{k_0}| = 0$)

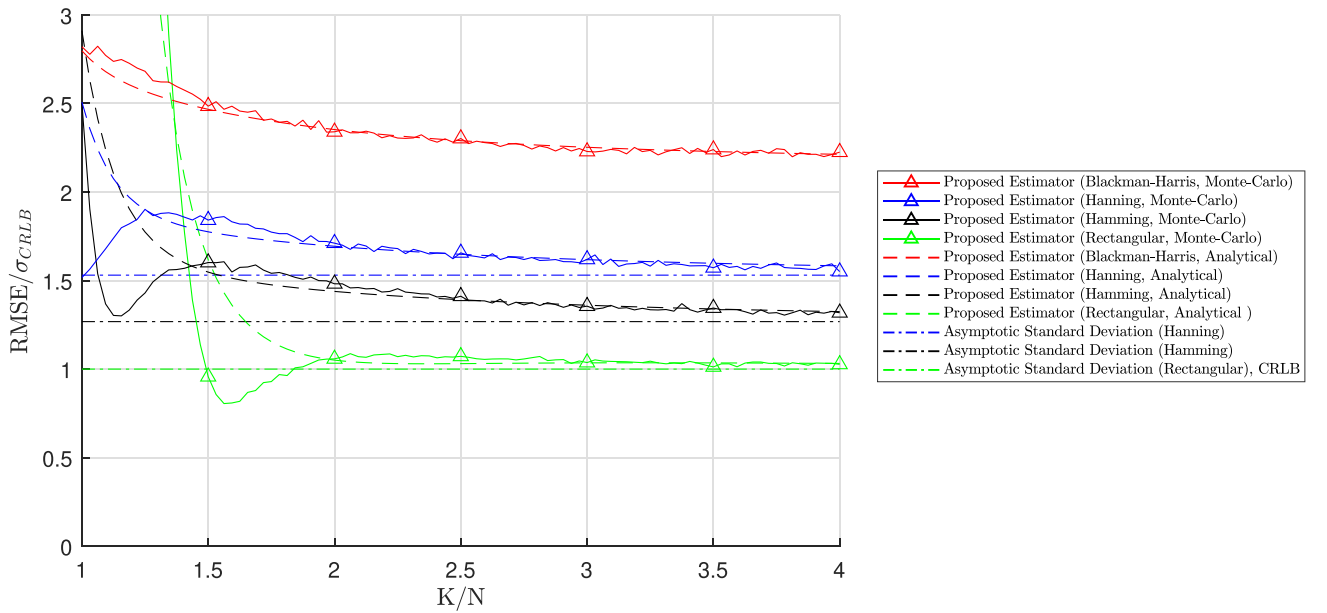


FIGURE 5 Performance of proposed estimator (Signal-to-Noise Ratio = -10 dB, $N = 1024$, $|\omega - \omega_{k_0}| = 0.5$)

Candan's estimators. More precisely, this colour indicates the ratio between the RMSE of the proposed estimator and the RMSE of the best of Quinn's or Candan's estimators. The ratio is expressed in decibel.

Then, roughly speaking, one can conclude that the proposed method exhibits improvement compared to Quinn's and Candan's estimators when using significant zero-padding lengths ($K \geq 2N$) and for small to moderate SNR, which is the most challenging case.

6 | CONCLUSION

In this paper, the two-step frequency estimator presented in [19], limited to $K = 2N$ and non-tapered data, has been extended to the case of zero-padded and tapered data with the class of cosine windows. This new estimator completes the toolbox available for engineers as presented in Figures 6–9 and allows to improve the estimation performance compared to state-of-the-art techniques when $K \geq 2N$.

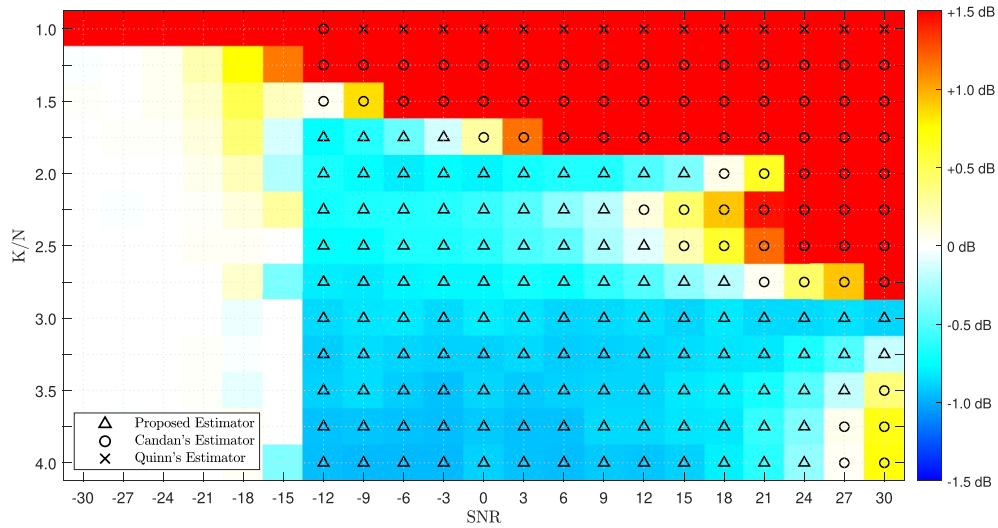


FIGURE 6 Comparison of the proposed estimator with Quinn's and Candan's estimators ($N = 1024$, rectangular window)

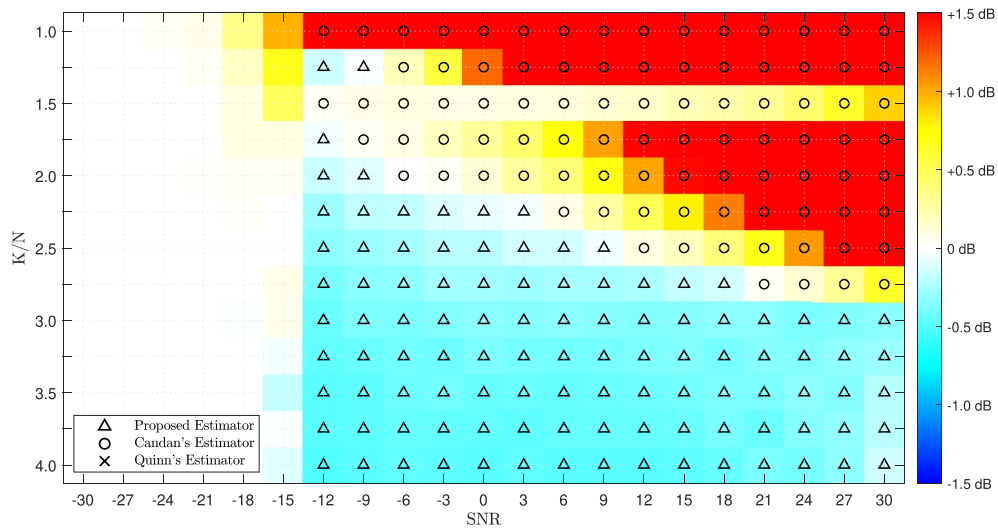


FIGURE 7 Comparison of the proposed estimator with Quinn's and Candan's estimators ($N = 1024$, Hamming window)

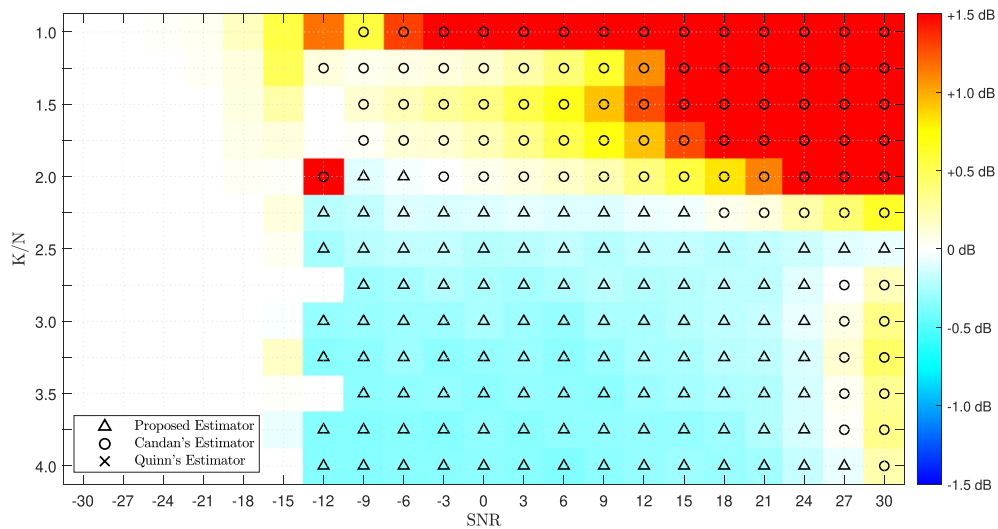


FIGURE 8 Comparison of the proposed estimator with Quinn's and Candan's estimators ($N = 1024$, Hanning window)

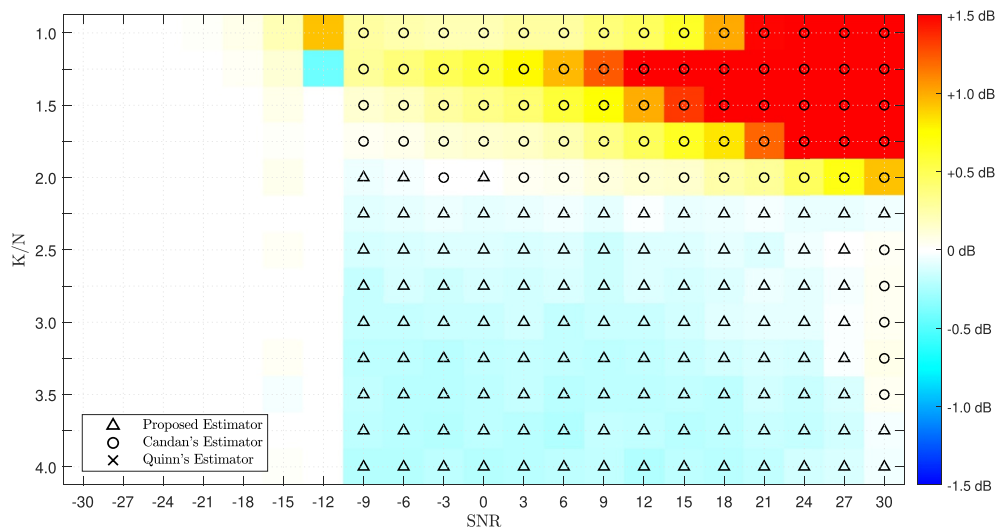


FIGURE 9 Comparison of the proposed estimator with Quinn's and Candan's estimators ($N = 1024$, Blackman–Harris window)

ACKNOWLEDGEMENTS

This research was supported by SpaceAble.

CONFLICT OF INTEREST

The authors declare that there is no conflict of interest.

DATA AVAILABILITY STATEMENT

Codes are available at <https://www.tesa.prd.fr>.

ORCID

Benjamin Gigleux  <https://orcid.org/0000-0001-5619-6848>

François Vincent  <https://orcid.org/0000-0002-7774-5428>

Eric Chaumette  <https://orcid.org/0000-0002-7029-3019>

REFERENCES

1. Renaux, A., et al.: On the high SNR CML estimator full statistical characterization. *IEEE Trans. Signal Process.* 54(12), 4840–4843 (2006)
2. Hannan, E.J.: The estimation of frequency. *J.Appl.PTrust.* 10(3), 510–519 (1973)
3. Rife, D.C., Boorstyn, R.R.: Single tone parameter estimation from discrete-time observations. *IEEE Trans. Inf. Theor.* 20(5), 591–598 (1974)
4. McMahon, A., Barret, R.F.: An efficient method for the estimation of the frequency of a single tone in noise from the phases of DFT. *Int. J. Adv. Comput. Sci. Appl.* 22(6), 101–106 (1986)
5. Macleod, M.D.: Fast nearly ML estimation of the parameters of real or complex single tones or resolved multiple tones. *IEEE Trans. Signal Process.* 46(1), 141–148 (1998)
6. Zakharov, Y.V., Tozer, T.C.: Frequency estimator with dichotomous search of periodogram peak. *Electron. Lett.* 35(19), 1608–160 (1999)
7. Aboutanios, E., Mulgrew, B.: Iterative frequency estimation by interpolation on fourier coefficients. *IEEE Trans. Signal Process.* 53(4), 1237–1242 (2005)
8. Aboutanios, E.: Generalised DFT-based estimators of the frequency of a complex exponential in noise. 2010 3rd International Congress on Image and Signal Processing, 16–18, 6, pp. 2998–3002. October 2010
9. Provencher, S.: Estimation of complex single-tone parameters in the DFT domain. *IEEE Trans. Signal Process.* 58(7), 3879–3883 (2010)
10. Brown, R.D., III, Liao, Y., Fox, N.: Low-complexity real-time single-tone phase and frequency estimation. *IEEE Military Communication* (2010)
11. Rife, D.C., Vincent, G.A.: Use of the discrete Fourier Trans_form in the measurement of frequencies and levels of tones. *Bell Syst.Tech. J.* 49(2), 197–228 (1970)
12. Quinn, B.G.: Estimating frequency by interpolation using fourier coefficients. *IEEE Trans. Signal Process.* 42(5), 1264–1268 (1994)
13. Quinn, B.G.: Estimation of frequency, amplitude, and phase from the DFT of a time series. *IEEE Trans. Signal Process.* 45(3), 814–817 (1997)
14. Quinn, B.G., Hannan, E.J.: *The Estimation and Tracking of Frequency.* Cambridge University Press, New York (2001)
15. Quinn, B.G.: Frequency estimation using tapered data. *IEEE Int. Conf. Acoust. Speech Signal Process.*, Toulouse, France (2006)
16. Quinn, B.G.: Recent advances in rapid frequency estimation. *Recent Adv.Rapid Freq.Estmin Digit. Signal Process.* 19(6), 942–948 (2009)
17. Duda, K.: DFT interpolation algorithm for Kaiser–Bessel and Dolph–Chebyshev windows. *IEEE Trans. Instrum. Meas.* 60(3), 784–790 (2011)
18. Jacobsen, E., Kootsookos, P.: Fast, accurate frequency estimators. *IEEE Signal Process. Mag.* 24(3), 123–125 (2007)
19. Yang, C., Wei, G.: A noniterative frequency estimator with rational combination of three spectrum lines. *IEEE Trans. Signal Process.* 59(10), 5065–5070 (2011)
20. Candan, C.: Analysis and further improvement of fine resolution frequency estimation method from three DFT samples. *IEEE Signal Process. Lett.* 20(9), 913–916 (2013)
21. Candan, C.: Fine resolution frequency estimation from three DFT samples: case of windowed data. *Signal Process.* 114(1), 245–250 (2015)
22. Duhamel, P., Hollmann, H.: Split radix FFT algorithm. *Electron. Lett.* 20(1), 14–16 (1984)
23. Harris, F.J.: On the use of windows for harmonic analysis with the Discrete fourier transform. *Proc. IEEE.* 66(1), 51–83 (1978)
24. Richards, A.M.: *Fundamentals of Radar Signal Processing*, 2nd ed, pp. 249–259. McGraw-Hill Education, New York (2014)

How to cite this article: Gigleux, B., Vincent, F., Chaumette, E.: Generalized frequency estimator with rational combination of three spectrum lines. *IET Radar Sonar Navig.* 1–9 (2022). <https://doi.org/10.1049/rsn2.12246>